

<https://helda.helsinki.fi>

---

## Nanostickers for cells : a model study using cell-nanoparticle hybrid aggregates

Brunel, Benjamin

2016

---

Brunel , B , Beaune , G , Nagarajan , U , Dufour , S , Brochard-Wyart , F & Winnik , F M  
2016 , ' Nanostickers for cells : a model study using cell-nanoparticle hybrid aggregates ' ,  
Soft Matter , vol. 12 , no. 38 , pp. 7902-7907 . <https://doi.org/10.1039/c6sm01450j>

---

<http://hdl.handle.net/10138/224632>

<https://doi.org/10.1039/c6sm01450j>

---

cc\_by

publishedVersion

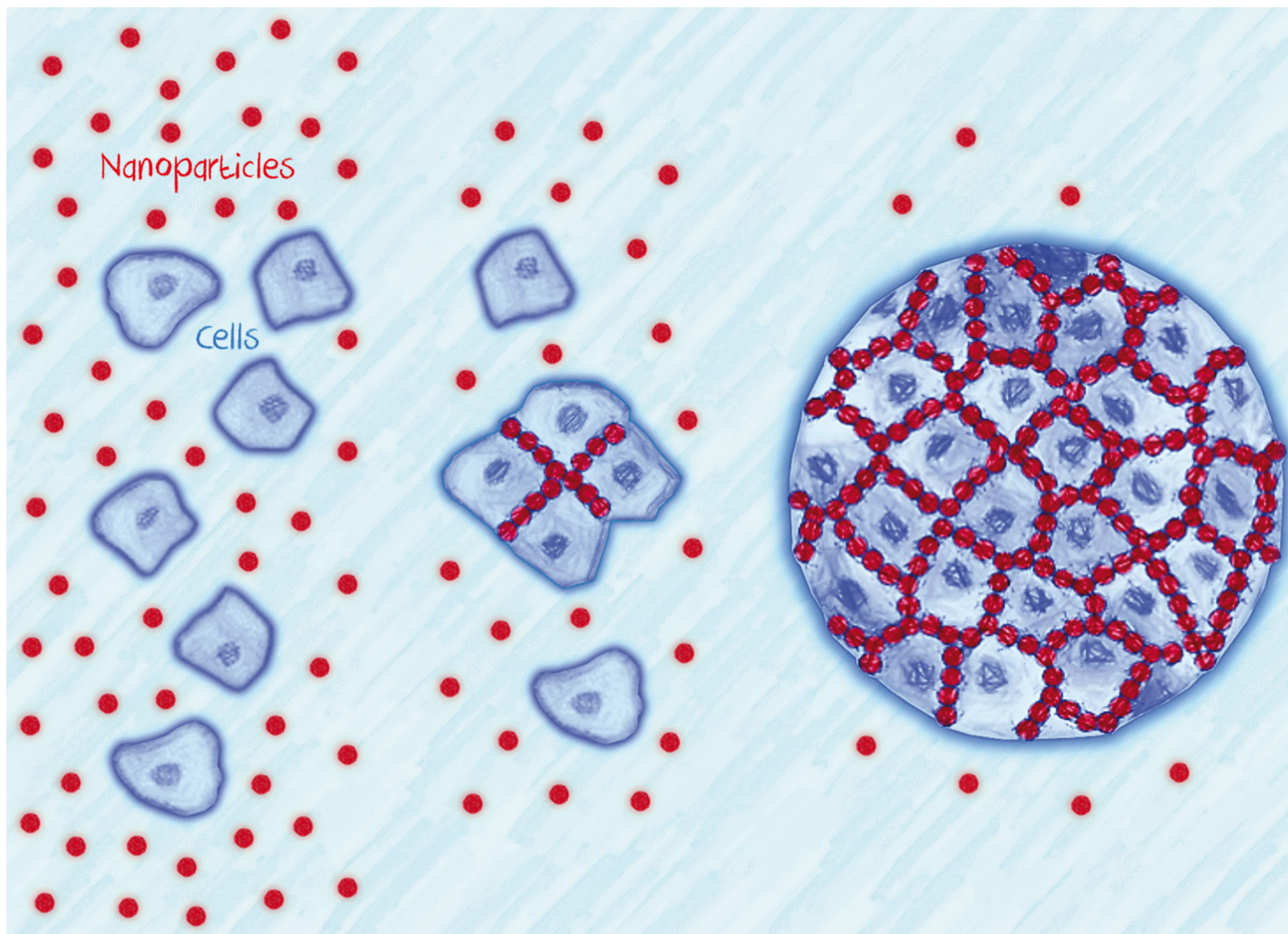
---

*Downloaded from Helda, University of Helsinki institutional repository.*

*This is an electronic reprint of the original article.*

*This reprint may differ from the original in pagination and typographic detail.*

*Please cite the original version.*

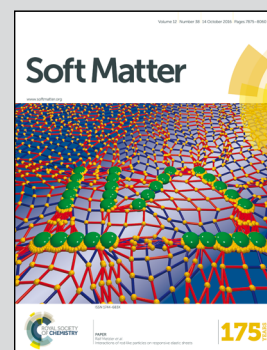


Highlighting research from the group of Professor Françoise M. Winnik\* in the WPI International Center for Materials Nanoarchitectonics (MANA), National Institute for Materials Science (NIMS), Tsukuba, Japan and of Professor Françoise Brochard-Wyart at Laboratoire de Physico Chimie Curie, Institut Curie, Paris, France. (\* also affiliated to the Department of Chemistry of the University of Montreal, Canada and the Department of Chemistry and Faculty of Pharmacy of the University of Helsinki, Helsinki, Finland.)

Nanostickers for cells: a model study using cell–nanoparticle hybrid aggregates

Nanoparticles are able to glue non-adhesive cells, leading to the formation of cellular aggregates by a mechanism of diffusion and collision. This allows us to define a “sticking efficiency parameter” for each type of nanoparticle, allowing us to select the most powerful ones.

As featured in:



See Françoise Brochard-Wyart, Françoise M. Winnik *et al.*, *Soft Matter*, 2016, 12, 7902.



[www.softmatter.org](http://www.softmatter.org)

Registered charity number: 207890



Cite this: *Soft Matter*, 2016, 12, 7902

Received 23rd June 2016,  
Accepted 31st August 2016

DOI: 10.1039/c6sm01450j

[www.rsc.org/softmatter](http://www.rsc.org/softmatter)

## Nanostickers for cells: a model study using cell–nanoparticle hybrid aggregates†

Benjamin Brunel,<sup>‡a</sup> Grégory Beaune,<sup>‡a</sup> Usharani Nagarajan,<sup>a</sup> Sylvie Dufour,<sup>bc</sup> Françoise Brochard-Wyart<sup>‡\*de</sup> and Françoise M. Winnik<sup>‡\*afg</sup>

**We present direct evidence that nanoparticles (NPs) can stick together cells that are inherently non-adhesive. Using cadherin-depleted S180 murine cells lines, which exhibit very low cell–cell adhesion, we show that NPs can assemble dispersed single cells into large cohesive aggregates. The dynamics of aggregation, which is controlled by diffusion and collision, can be described as a second-order kinetic law characterized by a rate of collision that depends on the size, concentration, and surface chemistry of the NPs. We model the cell–cell adhesion induced by the “nanostickers” using a three-state dynamical model, where the NPs are free, adsorbed on the cell membrane or internalized by the cells. We define a “sticking efficiency parameter” to compare NPs and look for the most efficient type of NP. We find that 20 nm carboxylated polystyrene NPs are more efficient nanostickers than 20 nm silica NPs which were reported to induce fast wound healing and to glue soft tissues. Nanostickers, by increasing the cohesion of tissues and tumors, may have important applications for tissue engineering and cancer treatment.**

Nanoparticles (NPs) are frequently used in nanomedicine and medical diagnostics where they serve as delivery agents, actuators, or imaging agents.<sup>1–3</sup> We discovered that bare nanoparticles can enhance cellular adhesion and mimic the specific homotypic interactions between membrane proteins, known as cadherins. The study was prompted by a report of Leibler *et al.* indicating that bare silica NPs can act as a glue for soft tissues, such as liver

sections,<sup>4</sup> and induce fast healing of deep wounds in the skin and liver of rats.<sup>5</sup> This new property of NPs hints that NPs could act as a cell/cell adhesive, but there has been no unequivocal demonstration of this phenomenon. We decided to carry out our study with cadherin-depleted mouse sarcoma S180 line cells to evaluate their cell assembly and aggregation.<sup>6</sup> S180 cells form weakly cohesive, small and rough aggregates, whereas transfected clones with a high level of cadherin expression form large cohesive aggregates that are very compact and smooth.<sup>7</sup> We demonstrate here that NPs can trigger the self-assembly of dispersed single cadherin-depleted cells into cohesive aggregates. We monitor the dynamics of aggregation, which are ruled by cell diffusion and cell–cell collision, and model the cell–cell adhesion induced by the NPs, or nanostickers, using a three-state dynamical model where the NPs are free, adsorbed on the membrane, or internalized by the cells.

The study was conducted as follows. First, we monitored the formation of S180 cell aggregates as a function of time in the absence of NPs and in the presence of NPs at a given concentration  $C_e$ . This first set of measurements gave us the “sticking efficiency parameter” ( $G$ ) of each type of NP. Then, we measured  $G$  versus the concentration of NPs. The dynamics of cell aggregation were modeled by analogy to the collision-induced aggregation of Brownian particles<sup>8</sup> that leads them to stick to each other with a probability  $P$  that depends upon cell–cell adhesion. This model leads to the definition of  $G$  as the normalized sticking probability. The nanosticker-induced cell–cell adhesion was evaluated using a three-state dynamical model, where NPs are either free in the cell culture medium, adsorbed on the cell membrane, or internalized. The most efficient nanostickers were identified by varying the model parameters. The study was conducted with silica NPs ( $\text{SiO}_2$ ) similar to those used by Leibler *et al.* and four types of polystyrene NPs, either negatively charged under physiological conditions, denoted as “Carbo” or positively charged, denoted as “Amine”. Their physico-chemical properties are listed in Table S1 (ESI†). The NPs selected were non-toxic to cells within the time and concentration domains of this study, as evaluated by the CCK-8 assay (see the ESI† for details). The polystyrene particles

<sup>a</sup> WPI International Center for Materials Nanoarchitectonics (MANA), National Institute for Materials Science (NIMS), 1-1 Namiki, Tsukuba, Ibaraki 305-0044, Japan. E-mail: Françoise.brochard-wyart@curie.fr, francoise.winnik@umontreal.ca

<sup>b</sup> Inserm, U955, Equipe 6, Créteil, 94000, France

<sup>c</sup> Université Paris Est, Faculté de Médecine, Créteil 94000, France

<sup>d</sup> Laboratoire Physico Chimie Curie, Institut Curie, PSL Research University, CNRS UMR168, 75005, Paris, France

<sup>e</sup> Sorbonne Université, UPMC Univ Paris 06, 75005, Paris, France

<sup>f</sup> Department of Chemistry and Faculty of Pharmacy, University of Montreal, CP 6128 Succursale Centre Ville, Montreal, QC H3C3J7, Canada

<sup>g</sup> Department of Chemistry and Faculty of Pharmacy, University of Helsinki, Helsinki, Finland

† Electronic supplementary information (ESI) available. See DOI: 10.1039/c6sm01450j

‡ These authors contributed equally to the manuscript.





were fluorescently labeled for the visualization of NP-treated cells by confocal fluorescence microscopy.

Aggregates of S180 cells were obtained using the hanging droplet method<sup>9</sup> (see the ESI† for experimental details). Droplets of the cell suspensions in the cell culture medium were deposited on a Petri dish cover. The cover was placed, inverted, on top of a container containing a phosphate buffer for humidity control. As time progresses, cells fall to the bottom of the droplets. They diffuse on this 2D surface and meet other cells. In the case of adherent cells, encounters result in the formation of groups of cells that adhere to each other to form clusters and, eventually, large aggregates. To monitor the progress of aggregate formation as a function of time, we prepared 7 covers, each holding 20 droplets of cell dispersion. The inverted covers were placed over the containers, and the 20 hanging droplets were collected at

various times over a period of 2 days. Each recovered droplet was placed on an untreated glass coverslip and observed by optical microscopy. Micrographs recorded at 15 min, 6 h, and 2 days after initiation of the study are presented in Fig. 1A, with cells alone, and Fig. 1B, with cells treated with Carbo20 NPs. Droplets collected at  $t = 15$  min contain only single cells whether Carbo20 NPs were added or not. After a period of 6 h, the droplet of S180 cells alone (A) presents mostly isolated cells, a few groups of 3 or 4 cells, and some larger clusters. In the case of cells treated with Carbo20 NPs (B) we observed clusters of cells and a few isolated cells. The total number of entities per unit area, circled in red, is named  $N$ . After a 2 day incubation, S180 cells alone (A) form a few loose clusters, surrounded by isolated cells and small groups, whereas the NP-treated cells aggregate in a single spheroid, approximately 250  $\mu\text{m}$  in diameter, surrounded by a few isolated cells.

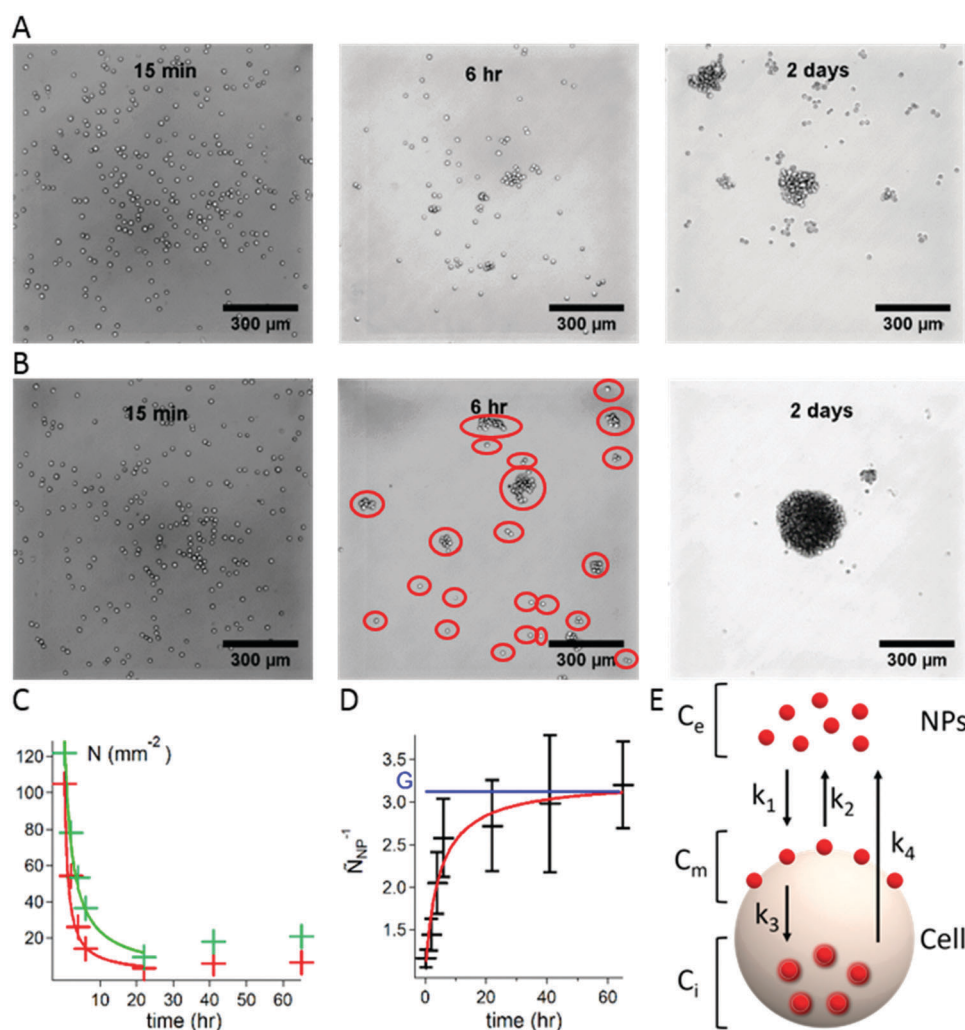


**Fig. 1** Formation of aggregates of S180 cells using the hanging droplet method. (A) Optical micrographs of droplets containing S180 cells collected 15 min, 6 h, and 2 days after initiation of the experiment. (B) Optical micrographs recorded under the same conditions in the case of a mixture of S180 cells and Carbo20 (volume fraction  $\phi_e = 5 \times 10^{-6}$  i.e.  $C_e = 4.7 \times 10^{11}$  NPs  $\text{mL}^{-1}$ ). The red circles highlight isolated entities defined as groups ( $N$ ). (C) Plot of the change with incubation time of the number of groups  $N$  per unit area observed in optical micrographs of droplets. Green data points and line: S180 cells alone; red data points and line: S180 cells with Carbo20 ( $\phi_e = 5 \times 10^{-6}$  i.e.  $C_e = 4.7 \times 10^{11}$  NPs  $\text{mL}^{-1}$ ). The lines are fits to the data using eqn (1). (D) Plot of the change with incubation time of  $N_{\text{NP}}^{-1}$  (Carbo20,  $\phi_e = 5 \times 10^{-6}$  i.e.  $C_e = 4.7 \times 10^{11}$  NPs  $\text{mL}^{-1}$ ). The blue horizontal line indicates the value of  $G$ ; the red line is the fit of the data points with eqn (2). Error bars represent the standard error over 20 drops. (E) Kinetic model describing the distribution of NPs between the bulk, the surface of the cell membrane, and the interior of the cell.



The number ( $N$ ) of groups per unit area was determined for a large number of micrographs collected over 70 h and plotted as a function of incubation time for S180 cells treated, or not treated, with NPs (see Fig. 1C, Carbo20 NPs). As time elapses, the number of groups ( $N$ ) decreases (the groups become larger). At very long times ( $t > 24$  h),  $N$  increases slightly as a consequence of cell division and subsequent rearrangement of cells into new aggregates.

The decrease of  $N$  with time was modeled as follows.<sup>10</sup> Once all the cells have fallen to the bottom of the drop, they diffuse on this surface with a mean diffusion rate  $V$ , such that a single cell (with a diameter  $d_{\text{cell}}$ ) covers a surface equal to  $V \cdot dt \cdot d_{\text{cell}}$  during the time interval  $dt$ . Thus, for  $N$  number of cells covering a surface area, a cell encounters an average of  $V \cdot dt \cdot d_{\text{cell}} \cdot N$  cells. We call the rate of collision  $K = V \cdot d_{\text{cell}}$ . If  $P$  is the probability for two cells to stick together, then  $K \cdot P$  is the rate of successful collisions. Progressively, cells form larger groups of cells ( $N$  is the number of groups per unit area), which obey the same dynamics, assuming  $K \cdot P$  to be independent of the size of the group. For a time period  $dt$ , each group fuses with  $P \cdot K \cdot dt \cdot N$  groups. It means that among the  $N$  groups,  $P \cdot K \cdot dt \cdot N \cdot N/2$  fusions occur. The evolution of  $N$  is governed by  $dN/dt = -PKN^2/2$ . After integration, the number of groups per unit area  $N(t)$  decreases as:

$$N(t) = N_0 / (1 + N_0 PKt/2) \quad (1)$$

The red line in Fig. 1C is the fit of the experimental values using eqn (1), knowing  $N_0 = 145 \text{ cells mm}^{-2}$ , and the fitting parameters:  $P_{\text{NP}}K = (5.5 \pm 0.4) \times 10^{-12} \text{ m}^2 \text{ s}^{-1}$  for the case of cells treated with NPs and  $P_{\text{control}}K = (2.0 \pm 0.1) \times 10^{-12} \text{ m}^2 \text{ s}^{-1}$  in the case of cells alone. Similar values for the rate of collision were measured by S. Douezan *et al.*<sup>10</sup> who studied the aggregation of S180 cells transfected to express E-cadherin on their surface diffusing on a non-adhesive substrate.

We can see from Fig. 1C that  $N$  decreases faster for cells treated with NPs. This is expressed in the fitting function by the difference between  $P_{\text{control}}$  and  $P_{\text{NP}}$ . The enhanced adhesion is quantified by the ratio of the probabilities  $P_{\text{NP}}/P_{\text{control}} = 2.8 \pm 0.3$ .

To compare the dynamics of aggregation with and without NPs, we design the ratio:

$$\tilde{N}_{\text{NP}}^{-1} = N_{\text{control}}/N_{\text{NP}} = (1 + N_0 P_{\text{NP}} Kt/2) / (1 + N_0 P_{\text{control}} Kt/2) \quad (2)$$

This ratio is plotted in Fig. 1D using data collected in the case of S180 cells treated with Carbo20 over a 3 day period. At long times,  $\tilde{N}_{\text{NP}}^{-1}$  tends to a plateau value, as predicted by eqn (2). The measurement of  $\tilde{N}_{\text{NP}}^{-1}$  after a given time provides the sticking efficiency parameter,  $G = P_{\text{NP}}/P_{\text{control}}$ , characteristic of a specific cell/NP pair. Several sets of measurements were carried at constant cell concentration ( $4 \times 10^4 \text{ cells mL}^{-1}$ ) varying the NP volume fraction from  $10^{-7}$  to  $10^{-5}$ . The change of  $G$  with NP concentration after two day (Fig. 2) presents two regimes (Fig. 2F): NPs have no effect on cell/cell adhesion ( $G = 1$ ) until their concentration exceeds a threshold,  $C_e^*$ . In this first concentration regime, NPs are internalized by cells, as confirmed by fluorescence imaging of S180 cells treated with NPs (Fig. S1, ESI†). For  $C > C_e^*$ , NPs are no longer internalized but adsorbed on the cell membrane. They promote cell adhesion characterized

by the cell-cell adhesion energy  $W_{\text{CC}}$ . This results in an increase of  $G$ , which reaches a plateau value,  $G_s$ , characterizing the sticking strength of each type of NP. The cell-cell adhesion energy  $W_{\text{CC}}$  as a function of NP surface concentration  $C_m$  can be written as  $W_{\text{CC}} = W_{\text{CC}}(0) + C_m U$ , where  $W_{\text{CC}}(0)$  is the adhesion energy in the absence of NPs and  $U$  is the energy gain per sticker.<sup>11,12</sup> The probability  $P_{\text{NP}}$  for cells to stick upon collision is proportional to  $e^{\beta[W_{\text{CC}}(0) + C_m U]}$ , where  $\beta$  is a numerical factor.  $G = P_{\text{NP}}/P_{\text{control}}$  can be written as  $e^{\beta[W_{\text{CC}}(0) + C_m U]} / e^{\beta W_{\text{CC}}(0)} = e^{\beta C_m U}$ . In the limit of  $\beta C_m U \ll 1$ , it leads to a linear relationship between  $G$  and  $C_m$ :  $G \approx 1 + \alpha C_m$ , with  $\alpha = \beta U$ .

The aim is to calculate  $C_m$  because the adhesive effect is due to the NPs located on the membrane. The spatial distribution of NPs is evaluated using the dynamical model shown in Fig. 1E. The NPs are located (i) in the bulk solution, with a concentration  $C_e$  assumed to be constant with time as the NPs are in excess; (ii) on the cell membrane, with a surface concentration  $C_m$ ; and (iii) internalized in the cell, with a concentration  $C_i$ . The internalization of NPs and their removal are crucial for therapeutic applications. The mechanisms of endocytosis and exocytosis of NPs are well described in ref. 13.

To describe the adsorption, the endocytosis and exocytosis of NPs in the cells, we introduce four rate constants defined in Fig. 1E:  $k_1$  and  $k_2$  associated with the adsorption and desorption of the NPs on the cell membrane,  $k_3$  with the internalization by endocytosis and  $k_4$  with the removal of NPs by exocytosis. From a dimensional analysis, we can write  $k_1 \approx r_p^3 \tau_{\text{on}}^{-1}$ , where  $\tau_{\text{on}}$  is the adsorption time;  $k_2 \approx \tau_{\text{off}}^{-1}$ , where  $\tau_{\text{off}}$  is the desorption time;  $k_3 \approx r_p^3 \tau_{\text{in}}^{-1}$ , where  $\tau_{\text{in}}$  is the internalization time; and  $k_4 \approx \tau_{\text{ex}}^{-1}$ , where  $\tau_{\text{ex}}$  is the exit time, which is assumed to be independent of  $r_p$ .

The kinetic equations determining the distributions of NPs and in particular  $C_m$  are:

$$dC_m/dt = k_1 C_e (C_{\text{ms}} - C_m) - k_2 C_m - k_3 C_m (C_{\text{is}} - C_i) \quad (3)$$

$$dC_i/dt = k_3 (A/V) C_m (C_{\text{is}} - C_i) - k_4 C_i \quad (4)$$

where  $k_i$  are the rate constants,  $C_{\text{ms}}$  and  $C_{\text{is}}$  are the saturating concentrations of NPs on the membrane and inside the cell, respectively,  $A$  is the cell membrane area, and  $V$  is the cell volume.

The ratio  $A/V$  in eqn (4) is associated with the transfer of the NPs from the surface into the cell volume and is equal to  $3/R$ , where  $R$  is the cell radius. The volume of the droplet is large compared to the volume of the cells and we can assume that  $C_e$  remains constant (Fig. S2, ESI†).

The internalized NPs are assumed to enter in the cell by endocytosis of the membrane decorated with NPs and to exit the cell by exocytosis are ruled by eqn (3) and (4). The stationary state leads to the NPs internalized concentration  $C_i$  and to the surface distribution of the NPs  $C_m$ .

In the stationary regime,  $dC_m/dt = 0$  and  $dC_i/dt = 0$ , which allow us to derive  $C_i$  and  $C_m$ .

$$k_1 C_e (C_{\text{ms}} - C_m) - k_2 C_m - k_3 C_m (C_{\text{is}} - C_i) = 0 \quad (5)$$

$$k_3 (A/V) C_m (C_{\text{is}} - C_i) - k_4 C_i = 0 \quad (6)$$



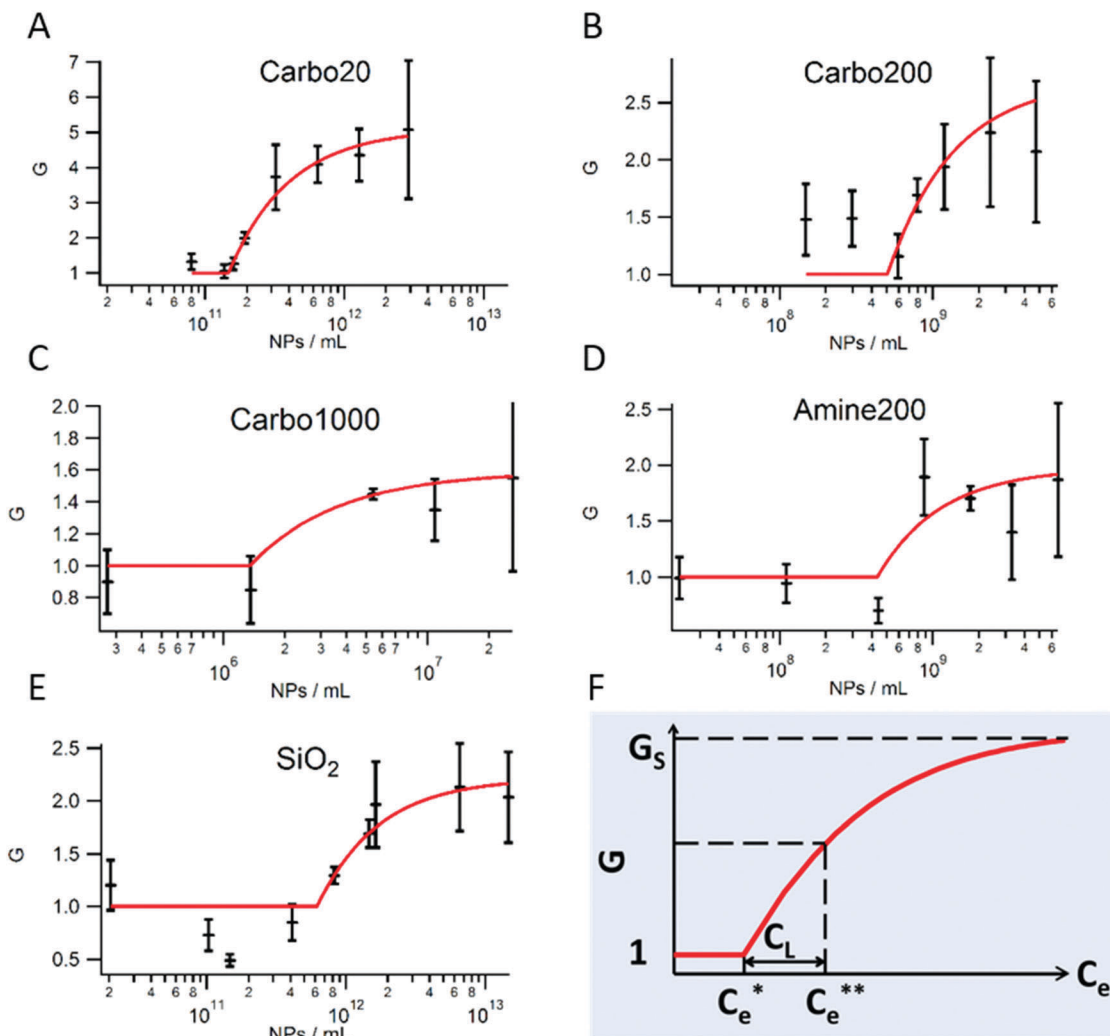


**Fig. 2** (A–E) Plots of the changes of  $G$  as a function of NP concentration expressed in number of NPs per unit of volume for S180 cells treated with different types of NPs; data points are shown in black; the red lines are the fits of the data using the 3-state model for the formation of aggregates with (A) Carbo20, (B) Carbo200, (C) Carbo1000, (D) Amine200 and (E) SiO<sub>2</sub>; (F) schematic representation of the plots of  $G$  vs. NP concentration indicating the characteristic concentrations used in the three-state model employed;  $C_e$ : NP concentration in numbers per volume unit;  $C_e^*$ : NP concentration corresponding to the internalization threshold;  $C_e^{**}$ : NP concentration corresponding to the threshold of saturation of the cell membrane surface;  $C_L$ : Langmuir concentration; error bars represent the standard error over 20 drops taken from the same Petri dish.

Combining eqn (5) and (6), leads to:

$$k_1 C_e (C_{ms} - C_m) - k_2 C_m - k_4 C_i R/3 = 0 \quad (7)$$

We derive  $C_i$  and  $C_m$  in the two regimes:

(I) Regime of internalization  $C_e < C_e^*$

In this regime, eqn (7) with  $C_m = 0$  leads to  $C_i = (3k_1/Rk_4)C_e C_{ms}$ .  $C_i$  increases up to  $C_{is}$  which defines the threshold concentration  $C_e^*$ .  $C_e^* = (Rk_4/3k_1)(C_{is}/C_{ms}) = (r_p^2/l^2)C_{is}$ , where  $r_p$  is the radius of the nanoparticles and  $l$  is a characteristic length defined by  $l^2 = 3k_1/Rk_4$  (in dimension,  $l^2 \approx (\tau_{ex}/\tau_{on})r_p^3/R$ ). The model leads to simple scaling laws for the threshold concentration  $C_e^*$ , where the NPs are internalized, that involves a characteristic length  $l$ . The measurement of  $l$  leads to a derivation of the exit time  $\tau_{ex}$  divided by the adsorption time,  $\tau_{on}$ .

(II) Regime of adsorption of the beads on the membrane  $C_e > C_e^*$

In this regime the cell is saturated with nanoparticles, and eqn (7) has to be written with  $C_i = C_{is}$ :

$k_1 C_e (C_{ms} - C_m) - k_2 C_m = (R/3)k_4 C_{is}$ . It leads to the solution for  $C_m$  given by:

$$C_m/C_{ms} = (C_e - C_e^*)/((C_e - C_e^*) + C_L) \quad (8)$$

where  $C_L = (k_2/k_1) + C_e^*$ .

Eqn (8) shows that this regime is ruled by a Langmuir law characterized by the Langmuir concentration  $C_L$ , but with a shift in the concentration  $(C_e - C_e^*)$ . When  $C_e - C_e^* > C_L$ , i.e.  $C_e > C_e^{**} = (k_2/k_1) + 2C_e^*$ ,  $C_m$  reaches the saturation value  $C_{ms}$  and  $G$  tends to  $G_s \approx 1 + \beta U C_{ms}$ . Assuming that the NPs are in close contact at saturation ( $C_{ms} = 1/(\pi r_p^2)$ ) and that  $\beta = A_c/k_B T$  ( $A_c$  being the contact area of colliding cells),  $G_s = 1 + n^* U/k_B T$ , where  $n^* = A_c C_{ms}$  is the number of NPs per cell-cell collision. By fitting the experimental efficiency parameter  $G(C_e)$  as shown



Table 1 Parameters  $C_e^*$ ,  $C_e^{**}$  and  $G_s$  for all tested types of particles

NP	$C_e^*$ [NPs mL <sup>-1</sup> ]	$\Phi_e^*$	$l^2/r_p^2$	$C_e^{**}$ [NPs mL <sup>-1</sup> ]	$G_s$
Carbo20	$1.5 \pm 0.1 \times 10^{11}$	$1.7 \times 10^{-6}$	$1.1 \pm 0.7 \times 10^3$	$2.6 \pm 0.5 \times 10^{11}$	$4.8 \pm 0.7$
Carbo200	$5 \pm 2 \times 10^8$	$1.5 \times 10^{-6}$	$1.3 \pm 0.5 \times 10^3$	$1.0 \pm 0.8 \times 10^9$	$2.7 \pm 0.8$
Carbo1000	$1.4 \pm 0.5 \times 10^6$	$9.4 \times 10^{-7}$	$2.1 \pm 0.8 \times 10^3$	$3 \pm 4 \times 10^6$	$1.6 \pm 0.4$
Amine200	$4.3 \pm 0.6 \times 10^8$	$1.8 \times 10^{-6}$	$1.1 \pm 0.3 \times 10^3$	$8 \pm 9 \times 10^8$	$2.0 \pm 0.5$
SiO <sub>2</sub>	$6 \pm 2 \times 10^{11}$	$3.9 \times 10^{-6}$	$0.5 \pm 0.4 \times 10^3$	$1.2 \pm 0.6 \times 10^{12}$	$2.2 \pm 0.4$

in Fig. 2 with this model we can obtain the 3 parameters  $C_e^*$ ,  $C_e^{**}$  and  $G_s$  for all types of particles. Their values are listed in Table 1.

#### 1 Internalization threshold concentration $C_e^*$

The value of the concentration  $C_e^*$  varies by five orders of magnitude when the size of the NPs increases from 20 to 1000 nm, whereas the volume fraction,  $\Phi_e^* = C_e^*(4/3)\pi r_p^3$ , is nearly the same for all types of NPs ( $\sim 1.5 \times 10^{-6}$ ). Hence, cells internalize a maximum volume of NPs, whatever the NP size.<sup>13</sup> From  $C_e^* = (r_p^2/l^2)C_{is}$  we deduce the characteristic length  $l$ , assuming that a cell digests a maximum volume fraction of particles equal to  $2 \times 10^{-3}$  derived from ref. 14.  $l^2/r_p^2$  is nearly constant ( $\sim 10^3$ ) for all types of NPs, which leads to an estimation of  $\tau_{ex}/\tau_{on}$  (of order  $10^6$  for  $r_p/R = 10^{-3}$ ).

#### 2 Surface saturation threshold concentration $C_e^{**}$

For all types of NPs,  $C_e^{**} \sim 2C_e^*$ , showing that  $k_2/k_1 \ll C_e^*$ .

#### 3 Sticking efficiency parameter $G_s$

Comparison between Carbo20, Carbo200 and Carbo1000 suggests that the cell-cell adhesion increases as the NPs' size decreases. Also a comparison between Amine200 and Carbo200 indicates that the charge has no influence on the sticking efficiency of NPs. The adhesive effect of SiO<sub>2</sub> used in [4] and [5] is not as strong as that of Carbo20 (Table S1b, ESI†). As discussed above,  $G_s = 1 + n^*U/k_B T$ . Assuming  $U \sim k_B T$ , we find that  $n^*$  is of order of few NPs.

To demonstrate that NPs mimic cellular adhesion molecules (CAMs) present on the surface of cohesive cells, we monitored *via* the same protocol, but without added NPs, the aggregation of LCAM cells, which are S180 cells transfected to express the highest level of cadherins.<sup>6</sup> The time dependence of  $N$ , the number of cell groups in a droplet (Fig. S3, ESI†), was determined and the experimental data were fitted with eqn (1) yielding the parameters  $N_0(65 \pm 5 \text{ cells mm}^{-2})$  and  $P_{LCAM}K[(4.2 \pm 0.6) \times 10^{-12} \text{ m}^2 \text{ s}^{-1}]$ . Using the  $P_{control}$  value obtained for S180 cells in the absence of NPs, we find  $G_{LCAM} = P_{LCAM}/P_{control} = 2.1 \pm 0.3$ . The  $G_{LCAM}$  values are of the same order of magnitude as  $G$  induced by NPs (Table 1). Hence, the methods developed for NPs could be applied also to quantify the adhesion between cells expressing different levels of CAMs on their membrane or differing by other types of modification of the cell membrane. This technique complements very well the classical dual pipette assay<sup>6</sup> used to measure cell-cell adhesion *via* detachment, because in the case of soft objects like cells, the energy of detachment can be a few orders of magnitude larger than the Dupré equilibrium adhesion energy.<sup>15</sup>

In conclusion, using a simple experimental protocol we have established that nanostickers are able to glue cells together and to increase the cohesion of the cells inside an aggregate.

As metastasis is often related to a decrease of cell-cell adhesion, nanostickers will reduce the escape of cells from tumors. They will also slow down the spreading of tumors, which results from a competition between cell-substrate and cell-cell adhesion. Experiments on the spreading of hybrid nanoparticle-cell aggregates and the characterization of their mechanical properties will allow us in the near future to demonstrate the role of nanostickers in the limitation of cancer proliferation. Moreover, beyond implementations in surgery already foreseen by Leibler *et al.*, hybrid cell/NP aggregates are unique constructs that may find applications in tissue engineering and cellular therapy. Most experiments on hybrid aggregates are related to mixtures of two types of cells leading to phase separation.<sup>16</sup> Hybrid aggregates of dead and living matter will open a new interesting field.

## Acknowledgements

The authors thank Dr J. Niskanen (University of Helsinki, Finland) for carrying out zeta measurements. This work was supported by the WPI-Program of the Ministry of Education, Culture, Sports, Science and Technology (MEXT), Japan, and by the NIMS "Nanotechnology Platform Project" also supported by MEXT. B.B. gratefully acknowledges financial support of his stay in MANA, NIMS, by the Ecole Normale Supérieure de Cachan (France).

## References

- O. Rabin, J. Manuel Perez, J. Grimm, G. Wojtkiewicz and R. Weissleder, *Nat. Mater.*, 2006, **5**, 118–122.
- A. Ito, M. Shinkai, H. Honda and T. Kobayashi, *J. Biosci. Bioeng.*, 2005, **100**, 1–11.
- X. Wang, Y. Wang, H. He, X. Chen, X. Sun, Y. Sun, G. Zhou, H. Xu and F. Huang, *J. Mater. Chem. B*, 2016, **4**, 779–784.
- S. Rose, A. Prevot, P. Elzière, D. Hourdet, A. Marcellan and L. Leibler, *Nature*, 2014, **505**, 382–385.
- A. Meddahi-Pellé, A. Legrand, A. Marcellan, L. Louedec, D. Letourneur and L. Leibler, *Angew. Chem., Int. Ed. Engl.*, 2014, **53**, 6369–6373.
- Y.-S. Chu, W. A. Thomas, O. Eder, F. Pincet, E. Perez, J. P. Thiery and S. Dufour, *J. Cell Biol.*, 2004, **167**, 1183–1194.
- S. Douezan, K. Guevorkian, R. Naouar, S. Dufour, D. Cuvelier and F. Brochard-Wyart, *Proc. Natl. Acad. Sci. U. S. A.*, 2011, **108**, 7315–7320.
- S. Douezan, J. Dumond and F. Brochard-Wyart, *Soft Matter*, 2012, **8**, 4578.
- P. Marmottant, A. Mgharbel, J. Käfer, B. Audren, J.-P. Rieu, J.-C. Vial, B. van der Sanden, A. F. M. Marée, F. Graner and



- H. Delanoë-Ayari, *Proc. Natl. Acad. Sci. U. S. A.*, 2009, **106**, 17271–17275.
- 10 S. Douezan and F. Brochard-Wyart, *Soft Matter*, 2012, **8**, 784.
- 11 P.-G. de Gennes, P.-H. Puech and F. Brochard-Wyart, *Langmuir*, 2003, **19**, 7112–7119.
- 12 G. I. Bell, M. Dembo and P. Bongrand, *Biophys. J.*, 1984, **45**, 1051–1064.
- 13 N. Oh and J. H. Park, *Int. J. Nanomed.*, 2014, **9**(1), 51–63.
- 14 C. Wilhelm, F. Gazeau, J. Roger, J. N. Pons and J.-C. Bacri, *Langmuir*, 2002, **18**, 8148–8155.
- 15 P. G. de Gennes, *Langmuir*, 1996, **12**, 4497–4500.
- 16 W. Song, C.-K. Tung, Y.-C. Lu, Y. Pardo, M. Wu, M. Das, D.-I. Kao, S. Chen and M. Ma, *Soft Matter*, 2016, **12**, 5739–5746.

